REPORT

Metazoan tRNA introns generate stable circular RNAs in vivo

ZHIPENG LU,[1] GRIGORY S. FILONOV,[2] JOHN J. NOTO,[3] CASEY A. SCHMIDT,[3] TALIA L. HATKEVICH,[3] YING WEN,[4] SAMIE R. JAFFREY,[2] and A. GREGORY MATERA[1,3,4,5,6]

[1]Department of Biology, University of North Carolina, Chapel Hill, North Carolina 27599, USA
[2]Department of Pharmacology, Weill Cornell Medical College, New York, New York 10065, USA
[3]Curriculum in Genetics and Molecular Biology, University of North Carolina, Chapel Hill, North Carolina 27599, USA
[4]Integrative Program for Biological and Genome Sciences, University of North Carolina, Chapel Hill, North Carolina 27599, USA
[5]Lineberger Comprehensive Cancer Center, University of North Carolina, Chapel Hill, North Carolina 27599, USA
[6]Department of Genetics, University of North Carolina, Chapel Hill, North Carolina 27599, USA

ABSTRACT

We report the discovery of a class of abundant circular noncoding RNAs that are produced during metazoan tRNA splicing. These transcripts, termed tRNA intronic circular (tric)RNAs, are conserved features of animal transcriptomes. Biogenesis of tricRNAs requires anciently conserved tRNA sequence motifs and processing enzymes, and their expression is regulated in an age-dependent and tissue-specific manner. Furthermore, we exploited this biogenesis pathway to develop an in vivo expression system for generating "designer" circular RNAs in human cells. Reporter constructs expressing RNA aptamers such as Spinach and Broccoli can be used to follow the transcription and subcellular localization of tricRNAs in living cells. Owing to the superior stability of circular vs. linear RNA isoforms, this expression system has a wide range of potential applications, from basic research to pharmaceutical science.

Keywords: circular RNA; expression system; noncoding RNA, ncRNA; tRNA processing

INTRODUCTION

The biosynthesis of tRNAs is remarkably complex (Phizicky and Hopper 2010). To begin with, eukaryotic tRNA genes typically contain internal RNA polymerase III (Pol III) promoters, wherein transcription actually initiates upstream of the control elements instead of downstream (Hofstetter et al. 1981). Once transcribed, maturation of pre-tRNAs requires cleavage of 5′ leader and 3′ trailer sequences, addition of CCA trinucleotides to the 3′ end, as well as a large number of base and sugar modifications throughout the body of the tRNA (Altman and Smith 1971; Guerrier-Takada et al. 1983; Castaño et al. 1985; Pellegrini et al. 2003; Gustilo et al. 2008; Phizicky and Hopper 2010; Torres et al. 2014). The extent and order of the different processing steps and their subcellular localization can vary between organisms (Wolin and Matera 1999; Phizicky and Hopper 2010). In addition, certain tRNA genes also carry intronic elements that must be removed in order to generate a functional RNA. Notably, tRNA introns are present in all three domains of life, and they usually occur within a select set of isoacceptor tRNA genes (Chan and Lowe 2009). Whereas bacterial tRNA introns are self-splicing ribozymes, the tRNA splicing endonuclease (TSEN) complex is responsible for cleavage of archaeal and eukaryotic tRNA introns (Abelson et al. 1998). Despite decades of studies on tRNA biogenesis, very little is known about the fate and function of tRNA introns. Studies in yeast have shown that tRNA introns are linear molecules (Knapp et al. 1979; Wu and Hopper 2014). In contrast, archaeal tRNA introns are known to be circularized following TSEN cleavage (Salgia et al. 2003; Danan et al. 2012). Whether tRNA introns from other eukaryotic species are linear, circular, or a mixture of both remains unclear.

Circular (circ)RNAs were once considered to be rare or aberrant transcripts (Nigro et al. 1991; Cocquerelle et al. 1992; Capel et al. 1993; Pasman et al. 1996). However, recent studies have shown that animal cells express tens of thousands of different circRNAs (Salzman et al. 2012, 2013; Hansen et al. 2013; Jeck et al. 2013; Memczak et al. 2013; Westholm et al. 2014). Most of the circRNAs reported to date are thought to have arisen during pre-mRNA splicing via a process called "back splicing" (Jeck et al. 2013), although 2′–5′ linked

Corresponding author: matera@unc.edu
Article published online ahead of print. Article and publication date are at http://www.rnajournal.org/cgi/doi/10.1261/rna.052944.115.

RNA circles can also accumulate by failure of intron debranching (Gardner et al. 2012; Zhang et al. 2013). During back splicing, the 3′ end of a downstream exon is ligated together with the 5′ end of an upstream exon of the same molecule (Jeck and Sharpless 2014), and this process is now considered to be an integral, regulated feature of eukaryotic gene expression programs (Wang et al. 2014). Despite their ubiquity, the functions of endogenous circRNAs are largely unknown (Hentze and Preiss 2013; Lasda and Parker 2014), and methods for generating and studying them in vivo are few and far between (Ford and Ares 1994; Zhang et al. 2014; Petkovic and Müller 2015).

RESULTS AND DISCUSSION

Recently, we developed a bioinformatic tool, called Vicinal, for the analysis of RNA sequencing (RNA-seq) reads that cannot be mapped end-to-end in the genome (Lu and Matera 2014). Using a modified version of this program, we discovered a large number of reads that map in a chiastic manner to a *Drosophila* tRNA gene, *CR31905*. That is, the 5′ and 3′ ends of each of these reads map to opposite ends of a large, highly conserved intron that bifurcates this unusual tRNA gene (Fig. 1A). This mapping pattern is best explained by circularization of the intron. Moreover, the density of the junction-spanning (Vicinal) reads is comparable to that of the conventionally mapped (Bowtie2) reads, suggesting that the predominant form of this intron is circular.

Intronic metazoan tRNA genes express stable circular transcripts

Whereas most metazoan tRNA genes are intronless, *CR31905* not only contains an intron but it is also an unusually large one. For comparison, a plot of tRNA intron sizes among various eukaryotic genomes is shown in Figure 1B. The predicted secondary structure of the *CR31905* intron is highly conserved among Drosophilids, as demonstrated by the large number of covariant base pairs (Fig. 1C). To confirm that this RNA is indeed circular, we performed three additional tests. First, we carried out reverse transcription (RT)-PCR using total RNA and four different primer pairs, two of which are divergent and two that are convergent (Fig. 1D). Consistent with expectations for a circular RNA, the divergent primer pairs were also able to generate PCR products. Moreover, we detected the presence of concatameric PCR products (Danan et al. 2012) that are known to form as a result of reverse transcription on circular templates (Fig. 1D). Similarly, we detected concatameric RNA-seq reads that are derived from introns of other fruit fly tRNA genes, for example, *CR32520* (Supplemental Fig. S1).

Second, we performed Northern blotting on total larval RNA using an oligoprobe that spans the putative circular junction. The probe detects a prominent band that migrates anomalously on denaturing polyacrylamide gels, running at ~200 nt in a 10% gel, and ~125 nt in a 6% gel (Fig. 1E). Equivalent results were obtained with an intronic oligoprobe. For the third test, we carried out RNase R digestion of total larval RNA followed by Northern blotting. As shown in Figure 1F, the presumptive circular RNA is resistant to digestion with RNase R, whereas the controls (U1 and U4 snRNAs) are sensitive. Collectively, these experiments demonstrate that splicing of the *CR31905* transcript generates a stable intronic RNA, termed tric31905, and that the predominant form of this molecule is circular.

To investigate whether additional tricRNAs are indeed present in the *Drosophila* transcriptome, we analyzed RNA-seq data sets and were able to identify reads that span the predicted circular junction for 13 of the 16 intron-containing tRNA genes (Supplemental Table S1; Supplemental Fig. S1). The other three tRNA genes contain very small introns (<21 nt) and, for technical reasons, such junction reads are expected to be underrepresented in cDNA sequencing libraries. Thus, while we have yet to detect all of them by RNA-seq, it is likely that tricRNAs are produced from all 16 intronic tRNA genes in *Drosophila*.

We examined expression of tric31905 over developmental time and found that its levels increase substantially from embryos to adults (Fig. 2A). In contrast, expression of the mature tRNA (Tyr_{GUA}) was relatively constant. Notably, tric31905 expression was slightly lower in adult females, perhaps because the ovary is such a large organ and expression levels in these tissues were relatively low (Fig. 2A). Consistent with their embryonic origin, Schneider2 cells also showed relatively low levels. Additional experiments will be required to determine if expression of tric31905 is actively regulated; it is possible that the RNA simply builds up over time in the organism, peaking in adults.

In Archaea and Eukarya, cleavage of tRNA introns is carried out by a highly conserved set of four proteins called the tRNA splicing endonuclease (TSEN) complex (Abelson et al. 1998; Salgia et al. 2003). TSEN recognizes a canonical bulge-helix-bulge (BHB) motif in the pre-tRNA, cleaving within the anticodon loop (Fig. 2B). In metazoa, ligation of the two exonic tRNA halves is thought to be carried out by a complex that contains RtcB-like proteins (Popow et al. 2011, 2014; Kosmaczewski et al. 2014). To determine whether RtcB is also important for formation of tricRNAs, we carried out RNA interference (RNAi) in vivo. Database analysis identified CG9987 as the putative *Drosophila* RtcB ortholog. Using the GAL4:UAS system (Dietzl et al. 2007), ubiquitous expression of dsRNA targeting CG9987 resulted in pupal lethality. Analysis of total larval and pupal RNA from these animals revealed a significant reduction in tric31905 expression, relative to controls (Fig. 2C). Despite the fact that the fruit fly genome contains 10 tRNA:Tyr_{GUA} genes (each of which bears an intron), expression of mature tRNA:Tyr_{GUA} was also reduced following depletion of CG9987 (Fig. 2C). These results provide strong support for the hypothesis that CG9987 is the *Drosophila* RtcB ortholog, and that this protein

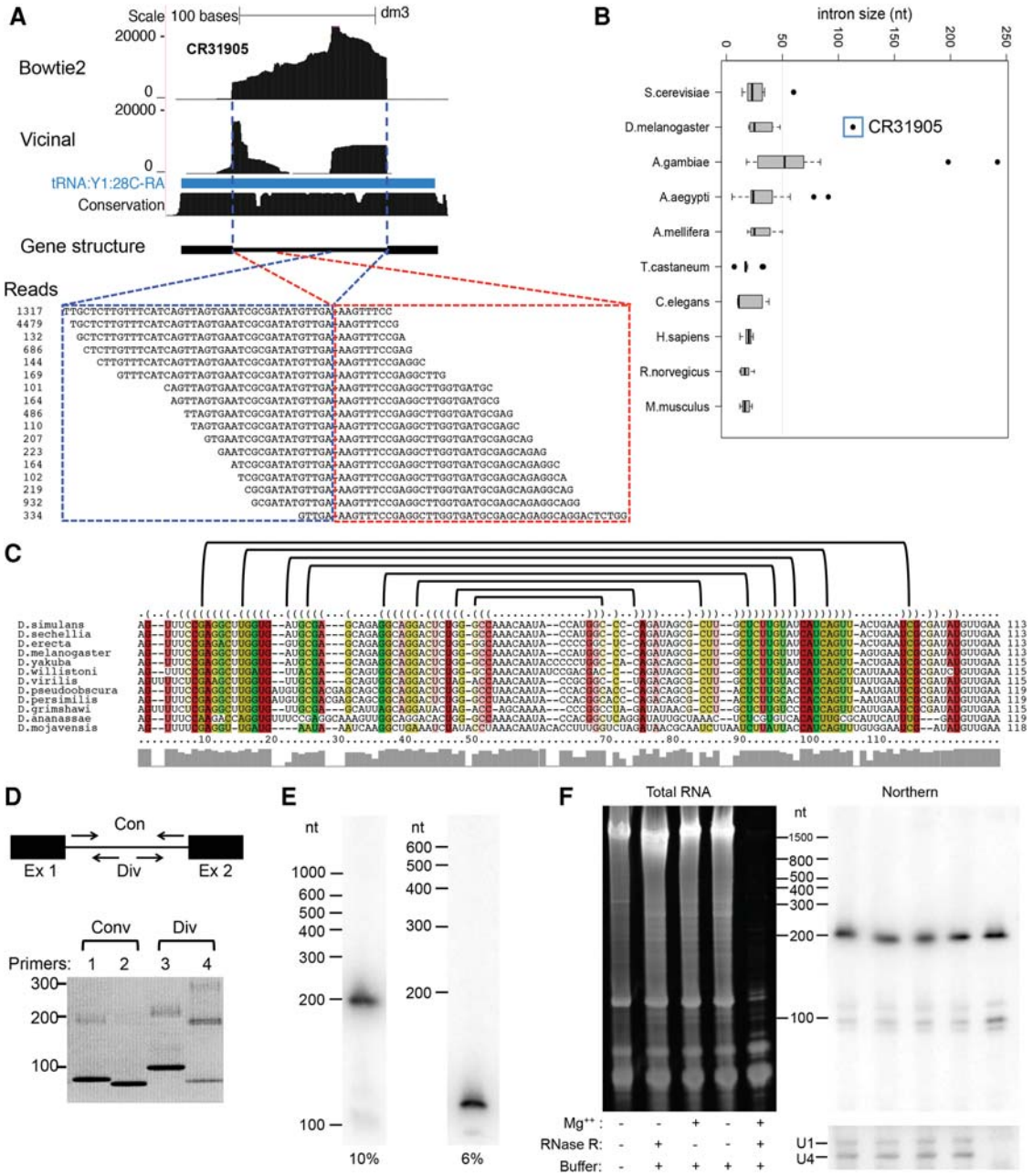

FIGURE 1. Detection of endogenous tricRNAs in *Drosophila melanogaster*. (*A*) RNA-seq reads spanning the circular junction of the intron of tRNA: Y1:28C-RA (tRNA:Tyr:GUA, CR31905). rRNA-depleted pharate adult RNA-seq data were mapped using Bowtie2 (for end-to-end and partially mapped reads) and a modified version of Vicinal (for circular junction-spanning reads). The structure of the pre-tRNA gene is shown under the tracks, with the thinner line representing the intron and the thicker lines representing the exons. The junction-spanning reads (counts ≥100) are shown *beneath* the gene structure. (*B*) Distribution of tRNA intron sizes among select eukaryotic genomes. The box plots show the first, second, and third quartiles; the whiskers represent a 1.5 interquartile range. Box thickness is proportional to the square root of the number of tRNA introns in each genome. Outliers are drawn as dots; the *Drosophila* CR31905 intron is marked by a blue box. The number of introns for each species is as follows: *Saccharomyces cerevisiae* 59, *D. melanogaster* 16, *Anopheles gambiae* 29, *Aedes aegypti* 32, *Apis mellifera* 11, *Mus musculus* 24, *Rattus norvegicus* 10, *Caenorhabditis elegans* 32, *Tribolium castaneum* 21, *Homo sapiens* 39. The plot was drawn using the boxplot R package. (*C*) Conservation of predicted secondary structure for tric31905 among Drosophilids. Sequences of the orthologous CR31905 tRNA intron from various species of *Drosophila* are shown. Note the compensatory base changes that maintain base-pairing within the predicted structure. (*D*) RT-PCR detection of tric31905 from total larval RNA. Cartoon shows schematic of an intronic tRNA gene with convergent (Con) and divergent (Div) primer pairs. Four pairs of primers (two Div and two Con) were tested. The ladders of PCR products correspond to amplification of concatemers of the cDNA via rolling circle reverse transcription. Experimental results agree well with the expected lengths (in base pairs) of the PCR products. Lane *1*: 82 + 113*n*; lane *2*: 75 + 113*n*; lane *3*: 100 + 113*n*; lane *4*: 78 + 113*n*; $n = 0, 1, 2, \ldots$ etc. (*E*) Abnormal migration of the 113-nt circular RNA tric31905. Total larval RNA samples were electrophoresed through 10% or 6% TBE-urea gels and tric31905 was detected by Northern blotting using a radiolabeled circular RNA junction oligomer. (*F*) Total larval RNA samples were treated with or without RNase R and run on a 10% TBE-urea gel. RNA was imaged using SYBR Gold (*left* panel), whereas tric31905 (*right upper* panel), U1 and U4 snRNAs (*right lower* panel) were detected by Northern blotting.

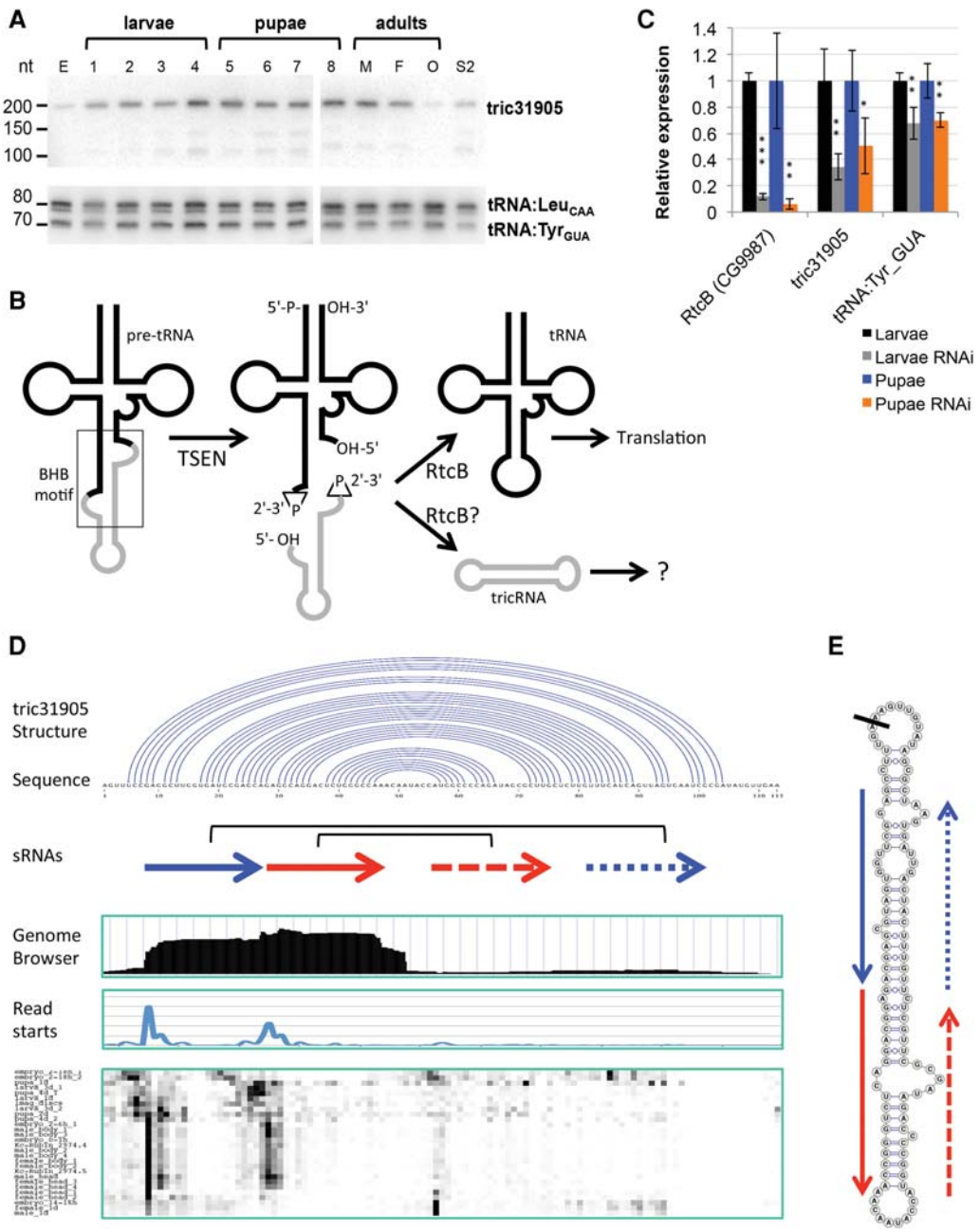

FIGURE 2. Expression and processing of tricRNAs. (*A*) Northern blot of tric31905 during fly development. tRNA:Leu$_{CAA}$ and tRNA:Tyr$_{GUA}$ were used as loading controls. (E) embryo, (1–4) 1- to 4-d-old larvae, (5–8) 1- to 4-d-old pupae, (M) male, (F) female, (O) ovary, (S2) S2 cells. (*B*) Cartoon of metazoan tRNA splicing and processing pathway illustrating the bulge-helix-bulge (BHB) splicing motif, tRNA splicing endonuclease (TSEN) cleavage sites (junctions of black and gray lines), 5′-OH and 2′,3′-cyclic phosphate groups. 5′ leader, 3′ trailer, and CCA nucleotides are not shown. In animal cells, RtcB is required for ligation of tRNA exons, but the intron ligase is unknown. (*C*) Knockdown of CG9987 reduces expression of tric31905 as well as that of mature tRNA:Tyr$_{GUA}$. RT-PCR was performed on total RNA samples from larvae or pupae. Error bars represent standard deviations from three biological replicates. (*) $P < 0.05$, (**) $P < 0.01$, (***) $P < 0.001$, Student's *t*-test. (*D*) Processing of tric31905 into small RNAs. Structure track: the predicted secondary structure of tric31905 in linear format. sRNAs track: diagram of the RNAs observed in small RNA-seq data. The solid arrows represent the most prominent species, whereas the dashed arrows represent the opposite strands. Genome Browser track: UCSC Genome Browser view of the read pileup (vertical scale 0–15,000). Read starts: numbers of reads starting at each position in the Genome Browser track (vertical scale: 0–15,000). Heatmap: the numbers of reads that start at each position for every small RNA-seq data set. Each row of the heatmap is normalized to a range of 0–1. (*E*) Cartoon showing locations of small RNAs along the secondary structure of tric31905, revealing a processing pattern similar to that of miRNAs.

is required for proper expression of mature tRNAs and tricRNAs.

Although endogenous tricRNAs have yet to be reported for any eukaryote, a ligase capable of circularizing chimeric archaeal/eukaryotic tRNA intron constructs in vitro is present in human cells (Englert et al. 2011; Popow et al. 2011). To determine whether eukaryotes other than *Drosophila* express tricRNAs, we analyzed a number of eukaryotic transcriptomes for tRNA circular junction reads (see Materials and Methods). Consistent with previous studies (Abelson et al. 1998), our analysis of budding yeast RNA-seq data suggest that yeast introns are exclusively linear (Supplemental Table S2). In most of the other RNA-seq data sets we analyzed, the tRNA introns are quite small and were therefore size-excluded from the cDNA library preparations. However, several metazoan genomes contain longer tRNA introns, ranging from ~40 to 250 nt (Fig. 1B). For example, an analysis of RNA-seq data sets from *C. elegans* identified junction-spanning reads for several tricRNAs (Supplemental Fig. S2). Thus, endogenous tricRNAs are easily detected in at least two distinct branches of Metazoa, nematodes, and arthropods. Given the high degree of conservation of the tRNA processing machinery, it is likely that tricRNAs are present in other animal species as well.

Tric31905 is predicted to form an evolutionarily conserved double-stranded structure (Fig. 1C), making it a potential substrate for the small RNA (sRNA) processing pathway. To determine whether tric31905 is processed into sRNAs, we analyzed published sRNA sequencing data sets (Berezikov et al. 2011). This analysis revealed prominent read pile-ups in a 45-nt region in the 5′ half of the intron (Fig. 2D, Genome Browser track), corresponding to one side of the duplex (Fig. 2D, tric31905 structure track). Inspection of read start positions within this pile of reads (Fig. 2D, sRNAs track) showed evidence of phased duplex production, with 2-nt 3′ overhangs. That is, the position where one abundant read ends is precisely where the next read begins, and the cuts are staggered. Such a pattern is generally taken as evidence for some sort of endonucleolytic cleavage event (e.g., dicing).

We then compared the profiles of small RNAs derived from tric31905 in various cell lines and developmental stages, and found that the phasing is present in most of the data sets, although the processing sites were not always precise (Fig. 2D, heatmap). Assuming that these small RNAs are indeed derived from the predicted duplex structure, the observed asymmetry is likely due to preferential association of one strand versus the other in a protein complex. Interestingly, in certain samples (e.g., embryo_14–16h, male_1d and female_1d), the opposite strands predominated, suggesting some type of mutually exclusive stabilization of a given strand of the duplex (Fig. 2D, heatmap). Additional experiments will be required to determine if any of these small RNAs are functional or if they represent distinct intermediates that are generated during normal degradation of circular tRNA introns.

An in vivo expression system for generating circular RNAs by tRNA splicing

To assay whether human cells can transcribe and process tricRNAs in vivo, we cloned two *Drosophila* intron-containing tRNA genes (CR31905, a tyrosine tRNA and CR31143, a leucine tRNA), transfected the native intron constructs (Fig. 3A) and harvested total RNA. Using qRT-PCR, we found that each produced readily detectable tricRNAs (Fig. 3B). We developed circular RNA expression vectors by removing the endogenous introns and replacing them with sequences that not only maintain the BHB motifs but also create convenient restriction sites for DNA subcloning (Fig. 3A,C). The resultant vectors are called pTRIC-Y and pTRIC-L (Y for tyrosine; L for leucine). To determine if pTRIC vectors can express heterologous tricRNAs, we inserted the Spinach2 RNA aptamer sequence (Strack et al. 2013), transfected the constructs into human cells, and carried out qRT-PCR analysis. Figure 3D shows that Spinach2 expression was readily detectable using divergent PCR primer pairs. Thus, human cells contain the requisite processing machinery to generate tricRNAs.

In addition to testing the processing of RNAs transcribed from internal tRNA promoters, we also generated a variety of constructs that feature external promoters (Fig. 3A). For these experiments, we used a novel in-gel imaging procedure to monitor transcription and intron circularization of another GFP-mimicking RNA aptamer, called Broccoli (Filonov et al. 2014). Samples were run on a denaturing polyacrylamide gel, renatured in the gel, and stained with DFHBI-1T to visualize Broccoli (Fig. 3E). Among those we tested, the human U6 snRNA promoter displayed the highest level of pre-tRNA transcription and tricRNA formation. In each lane, the shorter band is the presumptive Broccoli-tagged tricRNA and the longer band corresponds to the pre-tRNA transcript (Fig. 3E). The differences in the size of the longer band are due to the presence of variable 5′ leader sequences not included in the in vitro transcribed pre-tRNA control. RNase R treatment revealed that the pre-tRNA band is sensitive to digestion, whereas the circular tricRNA is refractive (Fig. 3E). We also tested whether or not inclusion of a specific U6 snRNA sequence within the 5′ tRNA leader might promote processing of the circular intron. This sequence, which is contained within the first 27 nt of the human U6 snRNA, is required for capping of the 5′ end of the transcript with a γ-monomethyl phosphate (Good et al. 1997). As shown in Figure 3F, the presence of these additional nucleotides at the 5′ end of the pre-tRNA resulted in a pronounced increase in tricRNA production (for each time point, compare lanes U6 to U6*). Quantification of band intensities 72 h post-transfection showed that the tricRNA to pre-tRNA ratio was ~1.5:1 for the U6 promoter, whereas it was ~10:1 for the U6* construct.

To assay the stability of tricRNAs, we transfected cells for 48 h and then treated them with Actinomycin D (ActD)

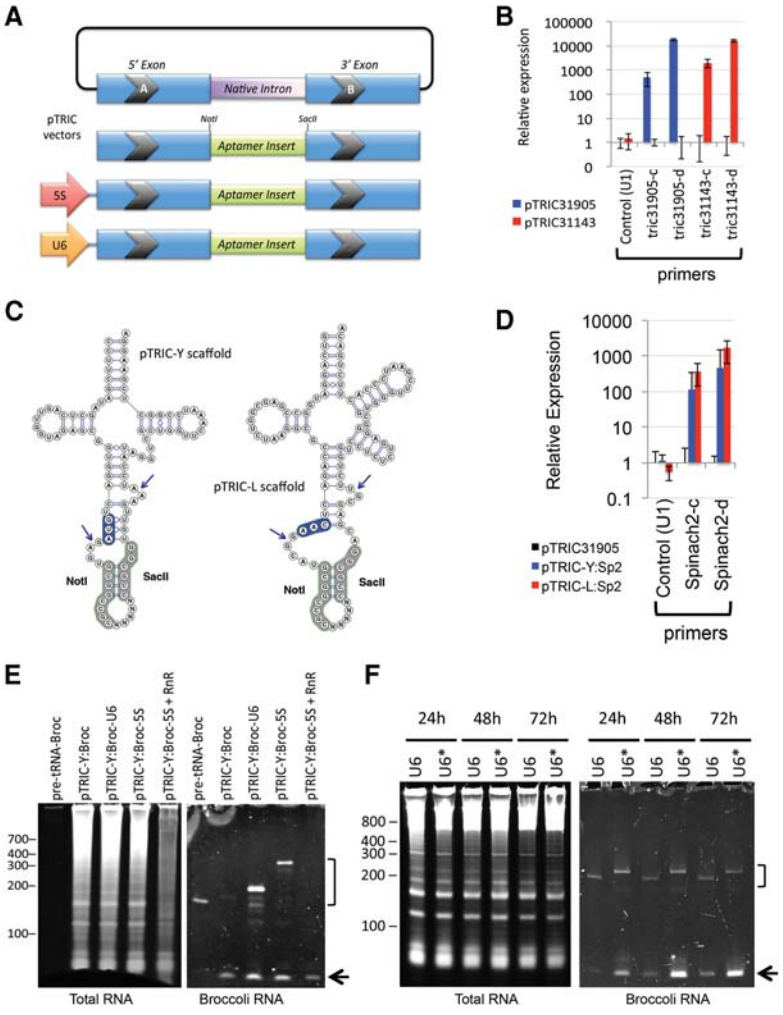

FIGURE 3. In vivo expression of stable, heterologous tricRNAs in human cells. (*A*) tricRNA vectors used for circular RNA expression, showing the tricRNA scaffold. The gray arrows represent the A and B boxes of the intragenic tRNA promoters. External 5S and U6 promoter constructs were also generated. (*B*) pTRIC31905 (tRNA:Tyr_{GUA}) and pTRIC31143 (tRNA:Leu_{CAA}) native intron vectors were transfected into HeLa cells for 24 h and their expression was measured by qRT-PCR. β-actin mRNA was used as normalization standard. U1 snRNA was used as a negative control (Control). tric31905-c and tric31143-c are convergent primer pairs, whereas tric31905-d and tric31143-d are divergent primer pairs used to measure expression of tric31905 and tric31143, respectively. Standard deviations were calculated from three biological replicates. (*C*) Secondary structures of RNAs expressed from pTRIC-Y and pTRIC-L scaffolds, highlighting the TSEN cleavage sites (arrows), anticodons (blue) and NotI–SacII restriction sites (gray). (*D*) Vectors for two circular Spinach2 constructs, pTRIC-Y:Sp2 (blue) and pTRIC-L:Sp2 (red), were transfected into HeLa cells and expression was determined using qRT-PCR. A control pTRIC31905 native intron vector was also used (black). The three experiments were analyzed using convergent (Spinach2-c) and divergent (Spinach2-d) primer pairs. β-actin mRNA was used as normalization standard and U1 snRNA was used as a negative PCR control (Control). Standard deviations were calculated from three biological replicates. (*E*) In-gel detection of Broccoli-tagged RNAs expressed from three different pTRIC-Y constructs bearing tRNA, U6 sRNA, or 5S rRNA promoters. HEK293T cells were transfected and total RNA was run on a 6% TBE-urea gel. The gel was washed to remove the urea, renatured in buffer, and stained with DFHBI-1T to reveal Broccoli (*right* panel), then stained with SYBR Gold to reveal total RNA (*left* panel). (RnR) RNase R treatment prior to gel electrophoresis. In vitro transcribed pre-tRNA-Broccoli (5 ng) was used as a positive control (first lane). In the experimental lanes, the *upper* bands (bracket) correspond to the precursor tRNAs; the *lower* band (arrow) corresponds to the mature circular Broccoli tricRNA. (*F*) Capping of the pre-tRNA improves production of circular RNAs. Two different U6 snRNA promoter constructs were tested, one that includes the first 4 nt of human U6 snRNA (U6) and a construct that includes the first 27 nt (U6*). HEK293T cells were transfected for the indicated times prior to harvesting total RNA. Electrophoresis, gel-detection, and band labels as described in *E*.

to halt new RNA synthesis for various lengths of time prior to harvesting RNA. As shown in Figure 4A,B, the pre-tRNA disappeared relatively rapidly, whereas the tricRNA was quite stable. Similar results were obtained using the pTRIC-L scaffold (Supplemental Fig. S3). Visualization of tricRNAs in vivo was carried out by cotransfection of cells with pTRIC-Y:Broc-U6 and mCherry constructs followed by flow cytometry (FACS) or fluorescence microscopy. FACS analysis revealed a large fluorescence enhancement over control (mCherry only) or nontransfected cells (Fig. 4C). Similar fluorescence profiles were obtained in untreated cells as compared with those that were treated for 2 h with ActD. However, epifluorescence microscopy revealed that the signal was primarily cytoplasmic in untreated cells, whereas in ActD treated cells the cytoplasmic localization was substantially reduced (Fig. 4D). Additional studies will be required in order to determine the extent to which ongoing transcription is required for transport of mature tricRNAs and/or their precursors to the cytoplasm.

Conclusions

We have identified a new class of metazoan circular RNAs and developed a system for their in vivo expression. Taken together, these findings illustrate the remarkable utility of tricRNA vectors, providing a means to express stable, high-copy, circular RNAs in human or other animal cells. The enhanced stability of tricRNAs makes them ideal candidates to serve as RNA-based effectors in biomedical research, synthetic biology, and biotechnology. Moreover, endogenous tricRNAs may well perform important cellular functions of their own. Future efforts in this area will be required in order to test this idea. However, given that defects in tRNA processing factors are known to cause neurodegenerative diseases (Budde et al. 2008; Weitzer et al. 2015), tricRNAs might also serve as important biomarkers of therapeutic agents aimed at restoring tRNA processing defects.

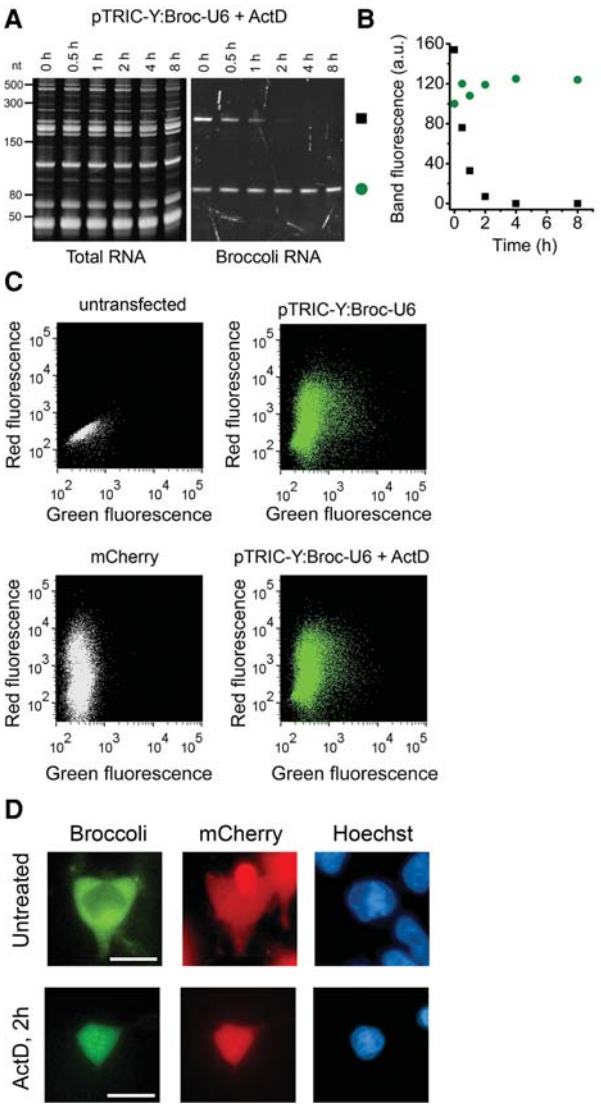

FIGURE 4. Stability and live-cell detection of fluorescent tricRNAs. (*A*) HEK293T cells were transfected with pTRIC-Y:Broccoli-U6, treated with actinomycin D (ActD) and harvested after the indicated times. Total RNA was run on a 10% TBE-urea gel, renatured, stained with DFHBI-1T for Broccoli (*right* panel) and then SYBR Gold for total RNA (*left* panel). (*B*) Quantification of linear and circular Broccoli RNA bands shown in *F*; (a.u.) arbitrary units. (*C*) Broccoli RNA detection by flow cytometry. HEK293T cells were transfected with either a mock or circular Broccoli-expressing plasmid (pTRIC-Y:Broc-U6). mCherry was also expressed from a separate plasmid as a transfection efficiency control (*y*-axis). In addition, Broccoli-tricRNA expressing cells were also treated with actinomycin D for 2 h before sorting. All cells were stained with DFHBI-1T and analyzed by flow cytometry in green and red channels. (*D*) Localization of circular Broccoli in living cells. Light microscopy of the same cells as described in *C*, stained with DFHBI-1T (Broccoli) and Hoechst. Scale bar, 20 µm.

MATERIALS AND METHODS

Mapping of circular junction-spanning reads

To extract reads spanning circular junctions, RNA-seq data sets were mapped to the *Drosophila* genome using Bowtie2 (Langmead and Salzberg 2012). However, since the default scoring function for bowtie2 is 20 + 8*ln(L) (corresponding to the default setting - -score-min G,20,8), and it requires at least a 26 nt perfect match in a 48-nt read, it misses reads mapped to the short tricRNAs (as short as 20 nt). In order to find the chimeric reads for the short tricRNAs, we used the following parameter settings for Bowtie2 in addition to the defaults: - -sensitive-local - -score-min G,9,8. The full list of parameter settings is bowtie2 - -sensitive-local - -score-min G,2,8 - -no-unal -x index_prefix -U filename.fastq -S filename.sam. The chimeric reads were mapped using a modified version of the Vicinal program, where two parts of the unmappable reads come from the same strand and are mapped in a chiastic manner (Lu and Matera 2014). At least 6 nt were required to map to each of the two ends of the intron for the reads to be counted. The modified program used for finding junction-spanning reads, Vicinal v3.0, is available at https://sites.google.com/site/zhipeng0426/programming.

Drosophila intron-containing tRNAs

The sequences for fly intron-containing tRNAs are listed here. The exons are in upper case while introns are in lower case.

CR31987
CCTTCGATAGCTCAGTTGGTAGAGCGGTGGACTGTAGattgggattacgaatgtagaCATCCATAGGTCGCTGGTTCAAATCCGGCTCGAAGGA
CR31986
CCTTCGATAGCTCAGTTGGTAGAGCGGTGGACTGTAGaagttttcagatctgatcacactttccaggtgatcgaatccagcaggcATCCATAGGTCGCTGGTTCAAATCCGGCTCGAAGGA
CR31905
CCTTCGATAGCTCAGTTGGTAGAGCGGTGGACTGTAGagtttccgaggcttggtgatgcgagcagaggcaggactctgggccaaacaataccatggccccagatagcgcttgctcttgtttcatcagttagtgaatcgcgatatgttgaaATCCATAGGTCGCTGGTTCAAATCCGGCTCGAAGGA
CR31435
CCTTCGATAGCTCAGTTGGTAGAGCGGTGGACTGTAGttggaaaaacatgcaatagaaATCCATAGGTCGCTGGTTCAAATCCGGCTCGAAGGA
CR31433
CCTTCGATAGCTCAGTTGGTAGAGCGGTGGACTGTAGttggaaaattatgcaatagaaATCCATAGGTCGCTGGTTCAAATCCGGCTCGAAGGA
CR31434
CCTTCGATAGCTCAGTTGGTAGAGCGGTGGACTGTAGttggaaaacatgcaatagaaATCCATAGGTCGCTGGTTCAAATCCGGCTCGAAGGA
CR31552
CCTTCGATAGCTCAGTTGGTAGAGCGGTGGACTGTAGttggaaaacaagcaatagaaATCCATAGGTCGCTGGTTCAAATCCGGCTCGAAGGA
CR31387
CCTTCGATAGCTCAGTTGGTAGAGCGGTGGACTGTAGttggcaaacaagcaatagaaATCCATAGGTCGCTGGTTCAAATCCGGCTCGAAGGA
CR32520
CCTTCGATAGCTCAGTTGGTAGAGCGGTGGACTGTAGatggtaaatcgcaatggcagagATCCATAGGTCGCTGGTTCAAATCCGGCTCGAAGGA
CR32525

CCTTCGATAGCTCAGTTGGTAGAGCGGTGGACTGTAGacggtt
tcatattgaatgcagaatacagagcagagATCCATAGGTCGCTGGTTCAA
GTCCGGCTCGAAGGA
CR32480
GCTCCAGTGGCGCAATTGGTTAGCGCACGGTACTTATAATca
gtattctgtgtgtatgagctatGCCGGGGTTGTGAGTTCGAGCCTCAC
CTGGAGCA
CR32481
GCTCCAGTGGCGCAATTGGTTAGCGCACGGTACTTATAATca
gtattctgtgtgtatatgagctatGCCGGGGTTGTGAGTTCGAGCCTCA
CCTGGAGCA
CR31143
GTCAGGATGGCCGAGCGGTCTAAGGCGCCAGACTCAAGgcat
tcagtcttgccctcgcagaagggcgtgtacgagcgTTCTGGTCCTCTCTGAG
GGCGTGGGTTCGAATCCCACTTCTGACA
CR32841
GTCAGGATGGCCGAGCGGTCTAAGGCGCCAGACTCAAGattt
aaaatcttactttctgaacgaaagcgtatgagcgTTCTGGTCCTCTCTGAGG
GCGTGGGTTCGAATCCCACTTCTGACA
CR30508
GTCAGGATGGCCGAGCGGTCTAAGGCGCCAGACTCAAGattg
aaaatcttactttctgaacgaaagtgtttgtgaatgagcgTTCTGGTCCTCTTTG
AGGGCGTGGGTTCGAATCCCACTTCTGACA
CR32127
GTCAGGATGGCCGAGCGGTCTAAGGCGCCAGACTCAAGagcg
aaagtctcttacctttcacagcaaggttcgattgagcgTTCTGGTCCTCTCTGA
GGGCGTGGGTTCGAATCCCACTTCTGACA

RNA secondary structures

Structured alignments of ncRNAs were carried out using LocARNA web server in the global standard alignment mode (Will et al. 2007). RNA secondary structures of the RNAs shown in this paper were predicted using the Vienna RNA package with default settings (Hofacker 2003). Manual adjustments were made where necessary to be consistent with the known physiological structures. Secondary structures were drawn using VARNA (Darty et al. 2009).

Prediction of tRNAs from genome sequences

tRNAscan-SE was used for the de novo prediction of tRNAs from genome sequences (Lowe and Eddy 1997; Schattner et al. 2005). The following parameters were specified that are different from the defaults: -L 500 -z 100. L is for the combined length of the variable loop and the intron, whereas *z* is the length of the padding sequence.

RNA-seq data sets

The following RNA-seq data sets were used in this study. Wild-type (Oregon R) early third instar larvae: EL Garcia, unpubl. Pharate adults: GSE50711 (four data sets) (Lu and Matera 2014). The ribominus total RNA-seq data for *S. cerevisiae* was downloaded from SRA with the accession number SRR1049520. Brief summary of the SRR1049520 library preparation: Total RNA was depleted of rRNA, fragmented by partial alkaline hydrolysis and then 27- to 40-nt fragments were used for library preparation. Reads were mapped to yeast genome sc3 using bowtie2 in the - -sensitive-local mode.

The following *C. elegans* RNA-seq data were downloaded from modENCODE and analyzed (Gerstein et al. 2010): N2 Yad-1 young adult (SRR316754-316755, ribominus 36 nt), four-cell embryo (SRR360132 DSN negative 50 nt, SRR360133 DSN positive 50 nt), DZ685 embryo Z1–Z4 cells (SRR578030, 50-nt DSN), N2 early embryo reference cells (SRR578031, 50-nt DSN), NW1229 larval L1 all neuron (SRR578032-578033, 50-nt DSN), N2 adult gonad (SRR578034, 50-nt DSN), LX837 larval L1 NSM neuron (SRR578035, 50-nt DSN), N2 early embryo (SRR578143, 50-nt ribo-zero), N2 larval L2 (SRR578144, 50-nt ribo-zero). A total of 10 intron-containing tRNAs from the *C. elegans* genome were extracted for generating the bowtie2 index, shown below (intron in lower case). The sizes of the introns range from 32 to 38 nt. The default scoring function was used for mapping the worm RNA-seq reads.

>LeuCAA1
GCACGGATGGCCGAGTGGTctAAGGCGCCAGACTCAAGcgtac
attgcttgcctcaagttcgaggttaactgggtgTTCTGGTACTCGTATGGGT
GCGTGGGTTCGAATCCCACTTCGTGCA
>LeuCAA2
GCACGGATGGCCGAGTGGTctAAGGCGCCAGACTCAAGcaata
gcttgcttcaagttcgaagccgattgggcgTTCTGGTACTCGTACGGGTGC
GTGGGTTCGAATCCCACTTCGTGCA
>LeuCAA3
GCACGGATGGCCGAGTGGTctAAGGCGCCAGACTCAAGcgtaa
cgcttacctcaagttcgaggtctactgggtgTTCTGGTACTCGTATGGGTG
CGTGGGTTCGAATCCCACTTCGTGCA
>LeuCAA4
GCACGGATGGCCGAGTGGTctAAGGCGCCAGACTCAAGcgaat
cgcttgcctcaagttcgaggtcaactgggtgTTCTGGTACTCGTATGGGTG
CGTGGGTTCGAATCCCACTTCGTGCA
>LeuCAA5
GCACGGATGGCCGAGTGGTctAAGGCGCCAGACTCAAGcaatt
gcttgcctcgagttcgaggtcgactgggtgTTCTGGTACTCGTATGGGTGC
GTGGGTTCGAATCCCACTTCGTGCA
>LeuCAA6
GCACGGATGGCCGAGTGGTctAAGGCGCCAGACTCAAGcgatt
gcttgcctcaagtacgaggtctcctgggtgTTCTGGTACTCGTATGGGTGC
GTGGGTTCGAATCCCACTTCGTGCA
>LeuCAA7
GCACGGATGGCCGAGTGGTctAAGGCGCCAGACTCAAGcgaaa
tgcttgcctcatgctcgaggtcgactgggtgTTCTGGTACTCGTATGGGTG
CGTGGGTTCGAATCCCACTTCGTGCA
>ThrUGU1
GGGCCTGTGGTGTAGTGGTtAACACACTGGTCTTGTGagtcgg
atttcatctcccggcttcaagttcaaAGCCAGAGACGTCGGTTCGAATC
CTTCCGGGTCCA
>ThrUGU2
GGGCCTGTGGTGTAGTGGTtAACACACTGGTCTTGTGagtcgg
atttcatctcccggcttcaagttcaaAGCCAGAGACGTCGGTTCGAATCC
TTCCGGGTCCA
>ThrUGU3
GGGCCTGTGGTGTAGTGGTtAACACACTGGTCTTGTGagtcgg
actttaaatcccggcttcaagttcaaAGCCAGAGACGTCGGTTCGAATC
CTTCCGGGTTTC

Analysis of small RNA-seq data sets

The sorted bam files for all the *Drosophila* small RNA expression profiling data generated by Lai and Hannon laboratories were downloaded from modENCODE (Berezikov et al. 2011), http://intermine.modencode.org/query/experiment.do?experiment= Small+RNA

+identification. The start positions of small RNA read clusters were extracted from the sorted bam files using the following samtools commands (an example data set is shown) (Li et al. 2009): samtools view modENCODE_xxxx_sorted.bam 2L:7711513-7711532 | cut -f4 | wc -l samtools view modENCODE_xxxx_sorted.bam 2L:7711533-7711552 | cut -f4 | wc -l. Starting positions of read counts were plotted using the Cluster 3.0 program (de Hoon et al. 2004).

RNA extraction and qRT-PCR

RNA extraction was performed using TRIzol reagent and cDNA was synthesized using SuperScript III (Life Technologies). Quantitative real-time PCR was performed in technical duplicates or triplicates, in addition to the biological triplicates, using Fermentas Maxima SYBR green qPCR kit (Thermo Fisher Scientific). All experiments were performed according to the manufacturer's instructions. The qRT-PCR primers were designed to have melting temperatures ~65°C so that the reactions could be performed at 60°C. Relative expression was determined using the $2^{-\Delta\Delta C_t}$ method (Livak and Schmittgen 2001).

Primers for testing tricRNA circularity

The following primers were used for testing the circularity of the tricRNAs. Note that in the primer names, *c* is convergent, *d* is divergent, *f* is forward, and *r* is reverse. tric31143cf: GCATT CAGTC TTGCC CTTCGC. tric31143cr: CGCTC GTACA CGCCC TTCT. tric31143df: AGAAG GGCGT GTACG AGCG. tric31143dr: GCGAA GGGCA AGACT GAATGC. PCR using both convergent and divergent primers for tric31143 generates 40-bp products. tric31905cf1: GGCTT GGTGA TGCGA GCAGAG. tric31905cf2: TGATG CGAGC AGAGG CAGGAC. tric31905cr1: ACTGA TGAAA CAAGA GCAAGCGC. tric31905df1: CGCTT GCTCT TGTTT CATCAGTT. tric31905dr2: CTGCC TCTGC TCGCA TCACCA. tric31905dr1: TGGTA TTGTT TGGCC CAGAGTC. tric31905cf1 and tric31905cr1 generates an 82-bp product. tric31905cf2 and tric31905cr1 generates a 75-bp product. tric31905df1 and tric31905dr1 generates a 100-bp product. tric31905df1 and tric31905dr2 generates a 78-bp product.

Northern blotting

RNA samples were electrophoresed through 6% or 10% TBE-urea gels (Life Technologies). Following electrophoresis, RNA was transferred to a nylon membrane. For the analysis of tricRNAs, the following oligonucleotides were 5′-end labeled with ^{32}P as probes for Northern blotting: tric31905cr1 and tric31905dr1 for tric31905; dmtRNALr1 for tRNA:Leu_{CAA} and dmtRNAYr1 for tRNA:Tyr_{GUA}. dmtRNALr1: GGGAT TCGAA CCCAC GCCCTC. dmtRNAYr1: GCCGG ATTTG AACCA GCGAC CTATG. See the next section for the rest of the sequences.

RNase R treatment of RNA samples and testing circularity of tricRNAs

Total RNA was isolated from third instar Oregon-R larvae using TRIzol reagent and dissolved in TE buffer. Equal amounts of RNA (10 µg) were mixed with 10× RNase R buffer, 10 U of RNase R (Epicentre Biotechnologies, Cat# RNR07250) and additional $MgCl_2$ to bring reactions to 1 mM [Mg^{2+}]. RNA samples were then incubated for 20 min at 37°C, after which they were electrophoresed in a 10% TBE-urea gel (Life Technologies). Gels were stained for total RNA and imaged. RNA was then transferred to a nylon membrane. The following oligonucleotides were 5′-end labeled and used as probes for Northern blotting: tric31905cr1, tric31905dr1, tric31905junction: AAGCC TCGGA AACTT TCAAC ATATCGC; U1 snRNA: GAATA ATCGC AGAGG TCAAC TCAGC CGAGGT; U6 snRNA: CTTCT CTGTA TCGTT CCAAT TTTAG TATAT GTTCT GCCGA AGCAAGA.

Developmental analysis of tricRNA expression

To analyze the expression of tricRNAs during fly development, fly embryos, larvae, pupae, adults, ovaries, and S2 cells were collected. The developmental samples were collected daily as follows: embryo, 1- to 4-d-old larvae, 1- to 4-d-old pupae, male adults, and female adults. The stages prior to eclosion were collected on a ~16-h window. Male and female adults were mixed ages. Ovaries were dissected from 2- to 6-d-old females. Samples were analyzed by Northern blot as described above.

Fly genetics and preparation of RNA samples

Two RNAi lines for *RtcB* (CG9987) were obtained from VDRC: line 36198 and line 36494. These two RNAi lines were crossed with an Actin-Gal4 driver to express the dsRNAs. Three samples were collected from each genotype and developmental stage. For VDRC36198 Actin-Gal4, VDRC36198/Tm3 (Tubby, without driver), VDRC36494 Actin-Gal4, and VDRC36494/Tm3 (Tubby, without driver), RNA was extracted from wandering third instar larvae and early-to-medium stage pupae. *RtcB* PCR primers are as follows: RtcB.f1, CGTCG GTGGA ACCAT GGGCA; RtcB.r1, AGATT GCGCC GGGAT TTGGCT.

Construction of the vectors expressing tric31143 and tric31905

To construct the pTRIC31143 and pTRIC31905 vectors expressing the genomically encoded tricRNAs, genomic DNA for tRNA CR31143 and tRNA CR31905 was cloned into the pDONR221 vector using the Gateway procedure (Life Technologies). The primers for cloning them are as follows, containing the attB1 and attB2 sequences, respectively. attB1.31143: GGGGA CAAGT TTGTA CAAAA AAGCA GGCT-ATAAA CGTGT TTTTG CGCCCCCA. attB2.31143: GGGGA CCACT TTGTA CAAGA AAGCT GGGT-ACAAA AAAAA ATTTG TCAGA AGTGG GATTC. attB1.31905: GGGGA CAAGT TTGTA CAAAA AAGCA GGCT-CATTT GGCCG ACCAA ATAGCGAC. attB2.31905: GGGGA CCACT TTGTA CAAGA AAGCT GGGT CCGAC AAAGA AAACG GAAGA AAACCC. Note that there is a single nucleotide polymorphism in the cloned CR31143 genomic DNA that is distinct from the genome reference (marked by parentheses): ATTCG TAA(G)A TGTCA GGATGGC. The variant in the reference genome is ATTCG TAA(C)A TGTCA GGATGGC. This variant does not affect the tRNA expression since it is outside of the tRNA gene, −3-nt upstream of the normal mature tRNA gene.

Construction of general vectors for circular RNA expression

pTRIC-Y and pTRIC-L (Y for Tyr and L for Leu) were constructed by performing NEB's Q5 site-directed mutagenesis on pTRIC31905 and pTRIC31143, respectively, according to manufacturer's protocol. The majority of intron sequences in pTRIC31905 and pTRIC31143 were replaced with NotI and SacII cloning sites while retaining intron sequences necessary for maintaining the splicing BHB motifs. The primers used for this cloning are as follows: Yf: CTCCG TAACT AGTTA CATCG TGGCC GCGGT GTTGA AATCC ATAGG TCGCT GGTT. Yr: CCATT TCATT CAGTT ACATC GCGGC CGCAC TCTAC AGTCC ACCGC TCTACC. Lf: CTCCG TAACT AGTTA CATCG TGGCC GCGGA CGAGC GTTCT GGTCC TCTCTG. Lr: CCATT TCATT CAGTT ACATC GCGGC CGCAT GCCTT GAGTC TGGCG CCTTA.

Construction of the vectors expressing circular RNA aptamers

pTRIC-Y:Sp2 and pTRIC-L:Sp2, which encode the Spinach2 RNA aptamer (Strack et al. 2013), were constructed by cloning Spinach2 from a vector using PCR amplification and appropriate primers with the restriction sites NotI and SacII on the 5′ and 3′ ends of Spinach2, respectively. The primer sequences are as follows: tric_Sp2NotIf: CTGTG CGGCC GCGAT GTAAC TGAAT GAAAT GGTGA AGGAC GGG. tric_Sp2SacIIr: CTGTC CGCGG CCACG ATGTA ACTAG TTACG GAGCT CACAC TCTAC T. pTRIC-Y: Broc and pTRIC-L:Broc, which encode the Broccoli RNA aptamer, were cloned in a similar manner. The following divergent primers were used for testing the circularity of circular Spinach2. tric_sp2_cf1: GATGT AACTG AATGA AATGG TGAAG GACGG. tric_sp2_cr1: GATGT AACTA GTTAC GGAGC TCACA CTCTAC. tric_sp2_df1: GTAGA GTGTG AGCTC CGTAA CTAGT TACATC. tric_sp2_dr1: CCGTC CTTCA CCATT TCATT CAGTT ACATC. PCR using the convergent primers generates a product of $(95 + 123n)$ bp ($n = 0, 1, 2, \ldots$). PCR using the divergent primers generates products of $(89 + 123n)$ bp from the pTRIC-L vector, and $(88 + 122n)$ bp from the pTRIC-Y vector.

Construction of tricRNA expression vectors with 5S and U6 promoters

To express tricRNAs under the control of external promoters, a three-way cloning approach was taken. First, the human 5S and U6 promoters were PCR amplified with a BamHI restriction site at the 5′ end and a SalI restriction site at the 3′ end. The sequences for the primers are as follows. 5SF: ATTAG GATCC GGCCC C. 5SR: ATTAG TCGAC GCCTA CAGC. U6F: ATTAG GATCC AAGGT CGGG. U6R: ATTAG TCGAC GCACG GTGTT TCGTC. Second, the tyrosine and leucine tRNA genes were PCR amplified with a SalI restriction site at the 5′ end and an XbaI restriction site at the 3′ end. The primer sequences are as follows: YF: ATTAG TCGAC TGGCC GACCA AATAG. YR: ATTAT CTAGA CCGAC AAAGA AAACG G. LF: ATTAG TCGAC TGCGC CCCCA. LR: ATTAT CTAGA ACAAA AAAAA ATTTG TCAGA AGT. Each PCR product was cut with the appropriate restriction enzymes (NEB) and column purified using a commercially available kit (Thermo Scientific). Third, the pAV vector was cut with BamHI and XbaI and gel purified using a kit (Thermo Scientific). The products were ligated using T4 DNA ligase (NEB), transformed into chemically competent cells, and screened for the proper inserts by sequencing.

Ectopic expression of circular RNAs

To express the endogenous and exogenous circular RNAs in cell culture, the plasmids were transfected into human HeLa cells or HEK 293T cells. Cells were maintained in DMEM supplemented with 10% FBS and penicillin/streptomycin at 37°C and 5.0% CO_2. Transfections of plasmids were conducted using Lipofectamine (Life Technologies) for HeLa cells or FuGENE HD (Promega) for HEK 293T cells following the manufacturer's protocol.

In-gel detection of fluorescent RNA aptamers

Total RNA from untransfected cells, circular Broccoli-expressing cells and from cells expressing 5S-fused Broccoli in a tRNA scaffold under the control of the 5S promoter (used as a positive control), was isolated using TRIzol LS reagent as per the manufacturer's instructions. RNA (4 µg) was loaded on a precast 6% TBE-Urea gel and run at 270–300 V in 1× TBE buffer. RiboRuler Low Range RNA Ladder (Thermo Scientific) was used to calibrate molecular weight. The position of Broccoli-containing bands can be visualized by staining the gel with DFHBI-1T, which specifically binds to Broccoli only, using a previously published method (Filonov et al. 2014). Briefly, after electrophoresis gels were washed 3×5 min with water and then stained for 30 min in 10 µM DFHBI-1T in a buffer containing 40 mM HEPES pH 7.4, 100 mM KCl, 1 mM $MgCl_2$. The gel was then imaged using a ChemiDoc MP imager (Bio-Rad) with 470 ± 30 nm excitation and 532 ± 28 nm emission. Next, to reveal all RNA in the lanes, the gel was again washed 3×5 min with water followed by staining for 30 min with SYBR Gold (Life Technologies) diluted 1/10,000 in TBE buffer. Then the gel was imaged with the same instrument using the SYBR Gold channel (302 nm excitation and 590 ± 110 nm emission). Gel band intensities were quantified using Image Lab 5.0 software (Bio-Rad). The 5S rRNA band was used for loading normalization.

Flow cytometry analysis of cells expressing circular Broccoli

HEK293T cells were transfected with the respective plasmids using FuGENE HD reagent (Promega) following the manufacturer's protocol. Empty pAV-U6 + 27 vector was used as a negative control. mCherry was expressed from pSuperior-mCherry as a transfection efficiency control. Eighty hours post transfection and 2 h before the analysis, the cells were treated with 5 µg/mL actinomycin D (or vehicle). Then the cells were harvested and resuspended in the 4% FBS/1× PBS solution containing 40 µM DFHBI-1T and kept on ice until analysis on the FACSAria II instrument (BD Biosciences). Transfected cells were analyzed in two channels: green (ex = 488 nm, em = 525 ± 25 nm) and red (ex = 561 nm, em = 610 ± 10). Processing and analysis of the data were performed in the FlowJo program (Tree Star).

In vivo imaging of Broccoli-tricRNA constructs

HEK293T cells were seeded on 3.5-cm glass-bottom dishes (MatTek Corporation) and then transfected with Broccoli- and mCherry-expressing plasmids. After ~72 h, the cells were treated with 5 µg/mL

actinomycin D (or vehicle) for 2 h. Twenty minutes before the imaging the cells were also treated with 20 μM of DFHBI-1T and 5 μg/mL Hoechst 33258. Live fluorescence images were taken with a CoolSnap HQ2 CCD camera through a 60× oil objective mounted on a Nikon Eclipse TE2000-E microscope and analyzed with the NIS-Elements software. The filter set used for Broccoli detection was a filter cube with excitation filter 470 ± 20 nm, dichroic mirror 495 nm (long pass), and emission filter 525 ± 25 nm. mCherry was detected using 560 ± 20 nm excitation filter, 585 nm (long pass) dichroic mirror, and 630 ± 37.5 nm emission filter. Hoechst-stained nuclei were imaged with 350 ± 25 nm excitation filter, 400 nm (long pass) dichroic mirror, and 460 ± 25 nm emission filter (all filters are from Chroma Technology). Exposure times: 500–1000 msec for Broccoli, 200 msec for mCherry and Hoechst. Background signals from cells expressing mock plasmid incubated with DFHBI-1T were subtracted from the corresponding images using NIS-Elements software (Nikon). Some Hoechst and mCherry images were γ corrected for better presentation.

SUPPLEMENTAL MATERIAL

Supplemental material is available for this article.

ACKNOWLEDGMENTS

We thank Drs. E. Garcia and E. Lai for helpful discussions and for sharing results prior to publication. C.A.S. was supported in part by a National Science Foundation Graduate Research Fellowship, DGE-1144081. T.L.H. was supported in part by a National Institutes of Health predoctoral traineeship, T32-GM007092. This work was supported by grants from the National Institutes of Health, R01-GM053034-18 (to A.G.M.) and R01-NS064516-07 (to S.R.J.).

Received June 22, 2015; accepted July 6, 2015.

REFERENCES

Abelson J, Trotta CR, Li H. 1998. tRNA splicing. *J Biol Chem* **273:** 12685–12688.

Altman S, Smith JD. 1971. Tyrosine tRNA precursor molecule polynucleotide sequence. *Nat New Biol* **233:** 35–39.

Berezikov E, Robine N, Samsonova A, Westholm JO, Naqvi A, Hung JH, Okamura K, Dai Q, Bortolamiol-Becet D, Martin R, et al. 2011. Deep annotation of *Drosophila melanogaster* microRNAs yields insights into their processing, modification, and emergence. *Genome Res* **21:** 203–215.

Budde BS, Namavar Y, Barth PG, Poll-The BT, Nürnberg G, Becker C, van Ruissen F, Weterman MA, Fluiter K, te Beek ET, et al. 2008. tRNA splicing endonuclease mutations cause pontocerebellar hypoplasia. *Nat Genet* **40:** 1113–1118.

Capel B, Swain A, Nicolis S, Hacker A, Walter M, Koopman P, Goodfellow P, Lovell-Badge R. 1993. Circular transcripts of the testis-determining gene Sry in adult mouse testis. *Cell* **73:** 1019–1030.

Castaño JG, Tobian JA, Zasloff M. 1985. Purification and characterization of an endonuclease from *Xenopus laevis* ovaries which accurately processes the 3′ terminus of human pre-tRNA-Met(i) (3′ pre-tRNase). *J Biol Chem* **260:** 9002–9008.

Chan PP, Lowe TM. 2009. GtRNAdb: a database of transfer RNA genes detected in genomic sequence. *Nucleic Acids Res* **37:** D93–D97.

Cocquerelle C, Daubersies P, Majérus MA, Kerckaert JP, Bailleul B. 1992. Splicing with inverted order of exons occurs proximal to large introns. *EMBO J* **11:** 1095–1098.

Danan M, Schwartz S, Edelheit S, Sorek R. 2012. Transcriptome-wide discovery of circular RNAs in Archaea. *Nucleic Acids Res* **40:** 3131–3142.

Darty K, Denise A, Ponty Y. 2009. VARNA: Interactive drawing and editing of the RNA secondary structure. *Bioinformatics* **25:** 1974–1975.

de Hoon MJ, Imoto S, Nolan J, Miyano S. 2004. Open source clustering software. *Bioinformatics* **20:** 1453–1454.

Dietzl G, Chen D, Schnorrer F, Su KC, Barinova Y, Fellner M, Gasser B, Kinsey K, Oppel S, Scheiblauer S, et al. 2007. A genome-wide transgenic RNAi library for conditional gene inactivation in *Drosophila*. *Nature* **448:** 151–156.

Englert M, Sheppard K, Aslanian A, Yates JR 3rd, Söll D. 2011. Archaeal 3′-phosphate RNA splicing ligase characterization identifies the missing component in tRNA maturation. *Proc Natl Acad Sci* **108:** 1290–1295.

Filonov GS, Moon JD, Svensen N, Jaffrey SR. 2014. Broccoli: rapid selection of an RNA mimic of green fluorescent protein by fluorescence-based selection and directed evolution. *J Am Chem Soc* **136:** 16299–16308.

Ford E, Ares M Jr. 1994. Synthesis of circular RNA in bacteria and yeast using RNA cyclase ribozymes derived from a group I intron of phage T4. *Proc Natl Acad Sci* **91:** 3117–3121.

Gardner EJ, Nizami ZF, Talbot CC Jr, Gall JG. 2012. Stable intronic sequence RNA (sisRNA), a new class of noncoding RNA from the oocyte nucleus of *Xenopus tropicalis*. *Genes Dev* **26:** 2550–2559.

Gerstein MB, Lu ZJ, Van Nostrand EL, Cheng C, Arshinoff BI, Liu T, Yip KY, Robilotto R, Rechtsteiner A, Ikegami K, et al. 2010. Integrative analysis of the *Caenorhabditis elegans* genome by the modENCODE project. *Science* **330:** 1775–1787.

Good PD, Krikos AJ, Li SX, Bertrand E, Lee NS, Giver L, Ellington A, Zaia JA, Rossi JJ, Engelke DR. 1997. Expression of small, therapeutic RNAs in human cell nuclei. *Gene Ther* **4:** 45–54.

Guerrier-Takada C, Gardiner K, Marsh T, Pace N, Altman S. 1983. The RNA moiety of ribonuclease P is the catalytic subunit of the enzyme. *Cell* **35:** 849–857.

Gustilo EM, Vendeix FA, Agris PF. 2008. tRNA's modifications bring order to gene expression. *Curr Opin Microbiol* **11:** 134–140.

Hansen TB, Kjems J, Damgaard CK. 2013. Circular RNA and miR-7 in cancer. *Cancer Res* **73:** 5609–5612.

Hentze MW, Preiss T. 2013. Circular RNAs: splicing's enigma variations. *EMBO J* **32:** 923–925.

Hofacker IL. 2003. Vienna RNA secondary structure server. *Nucleic Acids Res* **31:** 3429–3431.

Hofstetter H, Kressman A, Birnstiel ML. 1981. A split promoter for a eucaryotic tRNA gene. *Cell* **24:** 573–585.

Jeck WR, Sharpless NE. 2014. Detecting and characterizing circular RNAs. *Nat Biotechnol* **32:** 453–461.

Jeck WR, Sorrentino JA, Wang K, Slevin MK, Burd CE, Liu J, Marzluff WF, Sharpless NE. 2013. Circular RNAs are abundant, conserved, and associated with ALU repeats. *RNA* **19:** 141–157.

Knapp G, Ogden RC, Peebles CL, Abelson J. 1979. Splicing of yeast tRNA precursors: structure of the reaction intermediates. *Cell* **18:** 37–45.

Kosmaczewski SG, Edwards TJ, Han SM, Eckwahl MJ, Meyer BI, Peach S, Hesselberth JR, Wolin SL, Hammarlund M. 2014. The RtcB RNA ligase is an essential component of the metazoan unfolded protein response. *EMBO Rep* **15:** 1278–1285.

Langmead B, Salzberg SL. 2012. Fast gapped-read alignment with Bowtie 2. *Nat Methods* **9:** 357–359.

Lasda E, Parker R. 2014. Circular RNAs: diversity of form and function. *RNA* **20:** 1829–1842.

Li H, Handsaker B, Wysoker A, Fennell T, Ruan J, Homer N, Marth G, Abecasis G, Durbin R; 1000 Genome Project Data Processing Subgroup. 2009. The Sequence Alignment/Map format and SAMtools. *Bioinformatics* **25:** 2078–2079.

Livak KJ, Schmittgen TD. 2001. Analysis of relative gene expression data using real-time quantitative PCR and the $2^{-\Delta\Delta C_t}$ method. *Methods* **25:** 402–408.

Lowe TM, Eddy SR. 1997. tRNAscan-SE: a program for improved detection of transfer RNA genes in genomic sequence. *Nucleic Acids Res* **25:** 955–964.

Lu Z, Matera AG. 2014. Vicinal: a method for the determination of ncRNA ends using chimeric reads from RNA-seq experiments. *Nucleic Acids Res* **42:** e79.

Memczak S, Jens M, Elefsinioti A, Torti F, Krueger J, Rybak A, Maier L, Mackowiak SD, Gregersen LH, Munschauer M, et al. 2013. Circular RNAs are a large class of animal RNAs with regulatory potency. *Nature* **495:** 333–338.

Nigro JM, Cho KR, Fearon ER, Kern SE, Ruppert JM, Oliner JD, Kinzler KW, Vogelstein B. 1991. Scrambled exons. *Cell* **64:** 607–613.

Pasman Z, Been MD, Garcia-Blanco MA. 1996. Exon circularization in mammalian nuclear extracts. *RNA* **2:** 603–610.

Pellegrini O, Nezzar J, Marchfelder A, Putzer H, Condon C. 2003. Endonucleolytic processing of CCA-less tRNA precursors by RNase Z in *Bacillus subtilis*. *EMBO J* **22:** 4534–4543.

Petkovic S, Müller S. 2015. RNA circularization strategies in vivo and in vitro. *Nucleic Acids Res* **43:** 2454–2465.

Phizicky EM, Hopper AK. 2010. tRNA biology charges to the front. *Genes Dev* **24:** 1832–1860.

Popow J, Englert M, Weitzer S, Schleiffer A, Mierzwa B, Mechtler K, Trowitzsch S, Will CL, Lührmann R, Söll D, et al. 2011. HSPC117 is the essential subunit of a human tRNA splicing ligase complex. *Science* **331:** 760–764.

Popow J, Jurkin J, Schleiffer A, Martinez J. 2014. Analysis of orthologous groups reveals archease and DDX1 as tRNA splicing factors. *Nature* **511:** 104–107.

Salgia SR, Singh SK, Gurha P, Gupta R. 2003. Two reactions of *Haloferax volcanii* RNA splicing enzymes: joining of exons and circularization of introns. *RNA* **9:** 319–330.

Salzman J, Gawad C, Wang PL, Lacayo N, Brown PO. 2012. Circular RNAs are the predominant transcript isoform from hundreds of human genes in diverse cell types. *PLoS One* **7:** e30733.

Salzman J, Chen RE, Olsen MN, Wang PL, Brown PO. 2013. Cell-type specific features of circular RNA expression. *PLoS Genet* **9:** e1003777.

Schattner P, Brooks AN, Lowe TM. 2005. The tRNAscan-SE, snoscan and snoGPS web servers for the detection of tRNAs and snoRNAs. *Nucleic Acids Res* **33:** W686–W689.

Strack RL, Disney MD, Jaffrey SR. 2013. A superfolding Spinach2 reveals the dynamic nature of trinucleotide repeat-containing RNA. *Nat Methods* **10:** 1219–1224.

Torres AG, Batlle E, Ribas de Pouplana L. 2014. Role of tRNA modifications in human diseases. *Trends Mol Med* **20:** 306–314.

Wang PL, Bao Y, Yee MC, Barrett SP, Hogan GJ, Olsen MN, Dinneny JR, Brown PO, Salzman J. 2014. Circular RNA is expressed across the eukaryotic tree of life. *PLoS One* **9:** e90859.

Weitzer S, Hanada T, Penninger JM, Martinez J. 2015. CLP1 as a novel player in linking tRNA splicing to neurodegenerative disorders. *Wiley Interdiscip Rev RNA* **6:** 47–63.

Westholm JO, Miura P, Olson S, Shenker S, Joseph B, Sanfilippo P, Celniker SE, Graveley BR, Lai EC. 2014. Genome-wide analysis of *Drosophila* circular RNAs reveals their structural and sequence properties and age-dependent neural accumulation. *Cell Rep* **9:** 1966–1980.

Will S, Reiche K, Hofacker IL, Stadler PF, Backofen R. 2007. Inferring noncoding RNA families and classes by means of genome-scale structure-based clustering. *PLoS Comput Biol* **3:** e65.

Wolin SL, Matera AG. 1999. The trials and travels of tRNA. *Genes Dev* **13:** 1–10.

Wu J, Hopper AK. 2014. Healing for destruction: tRNA intron degradation in yeast is a two-step cytoplasmic process catalyzed by tRNA ligase Rlg1 and 5′-to-3′ exonuclease Xrn1. *Genes Dev* **28:** 1556–1561.

Zhang Y, Zhang XO, Chen T, Xiang JF, Yin QF, Xing YH, Zhu S, Yang L, Chen LL. 2013. Circular intronic long noncoding RNAs. *Mol Cell* **51:** 792–806.

Zhang XO, Wang HB, Zhang Y, Lu X, Chen LL, Yang L. 2014. Complementary sequence-mediated exon circularization. *Cell* **159:** 134–147.